Lab 1: Transducer Calibration & Pitot Wake Profiles

Gregory Golonka, Connor Hack, and Timothy Welch

February 2024

Abstract 1

Using a subsonic tunnel and a DAQ Unity computer, several tests were employed to measure the velocity profiles of a wind tunnel in the freestream, with a cylinder as a test article, and with a NACA 0015 airfoil at multiple angles of attack. Using the data collected, this report outlines the method by which the drag per unit span, coefficient of drag, and uncertainties in each were calculated and plotted, in addition to reporting and discussing those results. The drag of the cylinder was found to be $5.221 \pm 0.640 \frac{\text{N}}{\text{m}}$, which was significantly greater than the drag values of the airfoil. Although, both the drag values and drag coefficient values of the airfoil increased with the airfoil's angle of attack. Additionally, the uncertainty in each result was very reasonable with the very highest value of only 38.5%. The percent differences between expected and experimental coefficients of drag were also mostly reasonable for the airfoil. However, the percent difference in drag coefficient for the cylinder was 77.3%.

Abstract 2

This lab report delves into wind tunnel aerodynamics through a series of experiments: pressure transducer calibration, freestream velocity profiling, and wake profile analysis of a cylinder and a NACA 0015 airfoil. The pressure transducer calibration establishes a precise relationship between voltage and pressure difference, facilitating subsequent velocity measurements. Freestream velocity profiling reveals uniform flow characteristics within the wind tunnel, with velocities ranging from 24.75 to 25.05 m/s. Wake profiles of the cylinder and airfoil exhibit substantial velocity reductions behind the bodies, with the NACA 0015 airfoil experiencing a velocity drop from 25 to 23.5 m/s and the cylinder dropping to 20.9 m/s. Drag calculations, employing Riemann sum and Bernoulli's principle, yield drag coefficients for various angles of attack. Experimental drag coefficients, ranging from 0.010 to 0.036, show notable deviations from theoretical values, particularly at higher angles of attack. For instance, at 15 degrees angle of attack, the experimental drag coefficient is 0.036, compared to the theoretical value of 0.049. The results underscore the significant impact of body shape and angle of attack on drag characteristics, with the cylinder exhibiting higher drag compared to the airfoil across different angles of attack.

1 Introduction

This lab was broken up into three different experiments, each of which helped to improve understanding of experimental aerodynamics. The first objective of this lab was to calibrate a pressure transducer in order to measure the freestream velocity and flow. A pressure transducer is a device that converts a pressure measurement to a voltage for digital recording. The second objective was to measure the freestream velocity across the test section using a pitot probe. This experiment determined the flow uniformity across the y-axis. Finally, the last experiment analysed the drag of a cylinder and a two-dimensional airfoil by measuring their wake profiles using a pitot static probe. The objective was to use the data collected from all three experiments to create an accurate description of the drag profiles, including the uncertainties they have.

2 Experimental Setup

2.1 Define Ambient Conditions

Much of the later analysis relies on the ambient conditions of the laboratory, making it important to measure those conditions. The ambient pressure and temperature were obtained from a Fisher Scientific Traceable digital barometer within the testing room. This data was taken at both the beginning and end of the lab duration. The temperature and pressure data can be used to calculate the air density with the Ideal Gas Law given in the equation

$$\rho = \frac{P}{RT} \tag{1}$$

where ρ is the density, P is the ambient pressure, R is the specific gas constant of air taken to be 287 $\frac{\text{J}}{\text{kg}\cdot\text{K}}$, and T is the temperature. The values of P, T, and ρ taken and calculated for both times, as well as their averages, are tabulated in Table 1.

Table 1: Ambient conditions of the lab before and after the experiments.

Time	Temperature, T (K)	Pressure, P (Pa)	Density, ρ ($\frac{\text{kg}}{\text{m}^3}$)
5:30pm	296.5	9.95E+04	1.17
7:30pm	296.0	9.95E+04	1.17
Average	296.2 ± 0.6	9.95E+04 $\pm$ 400	1.17 ± 0.01

The uncertainties in these measurements are similarly important to the later analysis. The uncertainties in the average pressures, temperature, and density were calculated by propagating component uncertainties in quadrature. The component uncertainties from the above-stated measurement device are listed in Table 2.

Table 2: Error of pressure and temperature measurements.

Source	Pressure, ϵ_P (Pa)	Temperature, ϵ_T (K)
Reading	100	0.1
Systematic	400	0.4
Drift	100	0.4

The uncertainty in density was calculated from the quadrature addition of these uncertainties via the equation

$$\epsilon_\rho = \sqrt{\left(\frac{\epsilon_P}{RT}\right)^2 + \left(\frac{-\epsilon_T P}{T^2}\right)^2} \tag{2}$$

where ϵ_ρ is the uncertainty in density, ϵ_P is the uncertainty in pressure, and ϵ_T is the uncertainty in temperature.

2.2 Preparing Experiment

Before the experiment could be conducted, several steps had to be taken to ensure it ran smoothly. Once initial conditions were obtained, the subsonic tunnel used in the experiment was checked for debris and obstructions by objects or imperfections left in the tunnel. Then, the pitot probe, whose uncertainty is given by 14% of its range: 7E-03 V, was affixed to the mounting block within the tunnel with screws, utilizing the Allen wrenches provided in the lab. The pitot probe was positioned such that it was facing the inlet parallel to the flow. To allow for both the manometer and the pressure transducer to connect to the pitot probe, several tubes were connected:

- Each tube connected to a splitter
- High pressure tube connected to high pressure end of the manometer
- High pressure tube connected to the positive end of pressure transducer
- Low pressure tube connected to low pressure end of the manometer
- Low pressure tube connected to reference pressure end of pressure transducer

As the pitot static probe, manometer, and pressure transducers were already linked with splitting tubes by the previous group or by the TAs, checking that connections were secured was all that was required. Thus a simple test was employed by turning the motor speed to 25 Hz and observing the change in height of the manometer to ensure that there were no leaks.

A brief discussion of the wind tunnel used in this lab is also relevant. The lab was conducted using a turbine-type wind tunnel found in the Hessert Laboratories on the University of Notre Dame campus. Flow velocity was controlled within the tunnel by inputting a percentage of the maximum motor speed. The schematic for the wind tunnel can be found in

Figure 1. The schematic for the wind tunnel comes from the Lab 1 Transducer Calibration & Pitot Wake Profiles lab handout [1]. The schematic helps with a visual understanding for the discussion in Section 5.1.

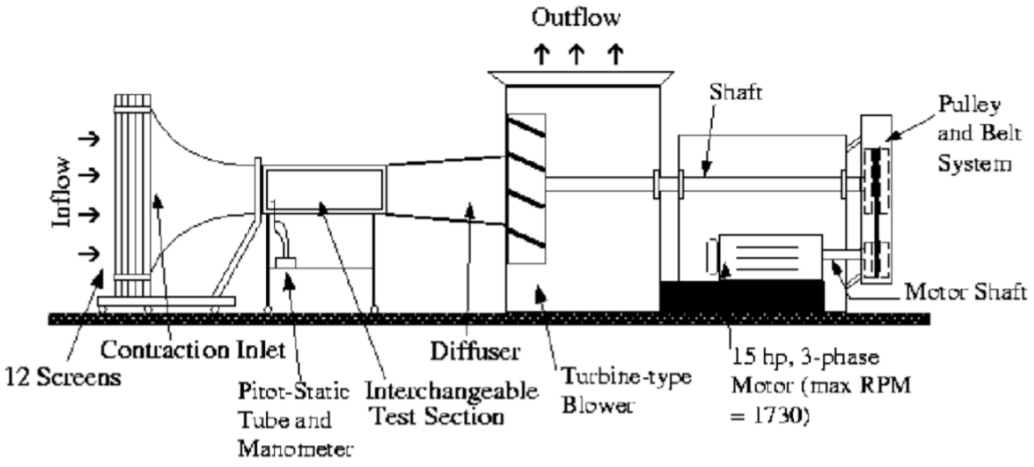

Figure 1: Informational graphic describing the different parts of a turbine-type wind turbine.

3 Experimental Procedure

The following procedure comes from the lab handout [1].

3.1 Pressure Transducer Calibration

Before the velocity profile of the freestream, cylinder, and airfoil could be collected, calibrating the system was required. To accomplish this, the pitot probe was positioned at $x = 15$ in. along the top of the tunnel. The DAQ Unity was employed to change the height of the pitot probe within the tunnel to $y = 0$ in. and read in data from the probe. With the manometer level, the tunnel speed was incrementally increased from 0% to 60% while the readings from the manometer and digital pressure transducer were recorded and fed into the DAQ Unity. After the test, the tunnel was set to 0%. The results from this pressure transducer calibration can be seen in 4.1 Results and Analysis.

3.2 Freestream Velocity Profile

After calibrating, the next test was to collect data on the freestream velocity profile. To obtain the velocity profile, the DAQ Unity moved the pitot tube to a new position of $y = -4$ in. within the tunnel. Once the pitot probe was in the correct position, the DAQ Unity was set to "enable analog in," 1000 number of steps, 31 repetitions, and positive direction. Once the wind tunnel was turned on to 45%, which corresponds roughly to 25 $\frac{\text{m}}{\text{s}}$ for the freestream velocity, the Unity read in the data gathered from the moving pitot probe

for the duration of the inputted commands. After the experiment, the tunnel was set to 0%. The results of the freestream velocity profile test can be found in 4.2 Results and Analysis.

3.3 Cylinder Wake Profiles

Freestream velocity data having been collected, the next test captured the wake profile of a cylinder. Before the tests were conducted, the cylinder profile was put into the test section of the wind tunnel. The tunnel speed was increased to 45% as it was in the freesteam velocity profile test. Similarly to the freestream velocity profile, the DAQ Unity moved the pitot tube to a new position of $y = -4$ in. within the tunnel. Then once the pitot probe was in the correct position, the DAQ Unity was set to "enable analog in," 500 steps, 63 repetitions, and positive direction. Just as in the freestream profile, once the wind tunnel was turned on, the Unity read in the data gathered from the moving pitot probe for the duration of the inputted commands. After the experiment, the tunnel was set to 0%. The final results from the cylinder wake profile tests can be found in 4.3 Results and Analysis.

3.4 Airfoil Wake Profile

The next test collected data on the wake profile of a NACA 0015 airfoil at multiple angles of attack. The cylinder used in the previous test was removed and a NACA 0015 airfoil was inserted into the center of the subsonic tunnel at 0° angle of attack. The pitot probe was set to $x = 36$ in. in the tunnel. At 0° angle of attack a course survey was conducted at 0.25 in. spacing to find the location of the wake. Within this region of interest, a fine survey at 0.05 in. spacing was conducted. With the fine survey completed, fine surveys were taken of 5, 10, and 15 degrees angle of attacks. After the experiment was conducted the tunnel speed was set to 0% The results for the 0, 5, 10, and 15 degree angle of attack profiles of the NACA 0015 airfoil can be found in 4.4 Results and Analysis.

4 Results and Analysis

4.1 Pressure Transducer Calibration

To convert the voltages outputted by the pressure transducer to actual pressure, a calibration was in order. The pressure transducer calibration was performed by applying a least square fit to the relationship between the voltage signal outputted to the computer and the pressure difference as measured by the inclined manometer. The result of the least squares regression was a linear relationship between voltage and pressure difference given by

$$\Delta P = 1.006 \left(\frac{\text{in.H}_2\text{O}}{\text{V}} \right) \cdot V + 0.011(\,\text{in.H}_2\text{O}) \tag{3}$$

where ΔP is the difference in pressure given in $\frac{\text{in.H}_2\text{O}}{\text{V}}$ and V is the voltage given in volts. Standard deviation data was also propagated through least squares regression using methods described in the Lab 1: Pre-Lab Assignment [2]. The standard deviations in the slope, a, intercept, b, and fitted pressure, y, are tabulated in Table 3.

Table 3: Standard deviation of least squared regression for pressure transducer calibration.

σ_a ($\frac{\text{in.H}_2\text{O}}{\text{V}}$)	σ_b (in.H_2O)	σ_y (in.H_2O)
0.0079	0.010	0.019

It is valuable to visualize the calibration data with their best fit and uncertainties. The measured data alongside the best-fit line with error bars—both vertical and horizontal—and confidence bounds of one standard deviation are plotted in Figure 2. Notably, the error bounds in Figure 2 are so minuscule that they are practically invisible given the scale of the range of data gathered. Nevertheless, basic inspection shows that the best fit for the calibration data is incredibly accurate, as reported by the correlation coefficient, R, visible in the legend of Figure 2, which is incredibly close to its maximum value of 1.

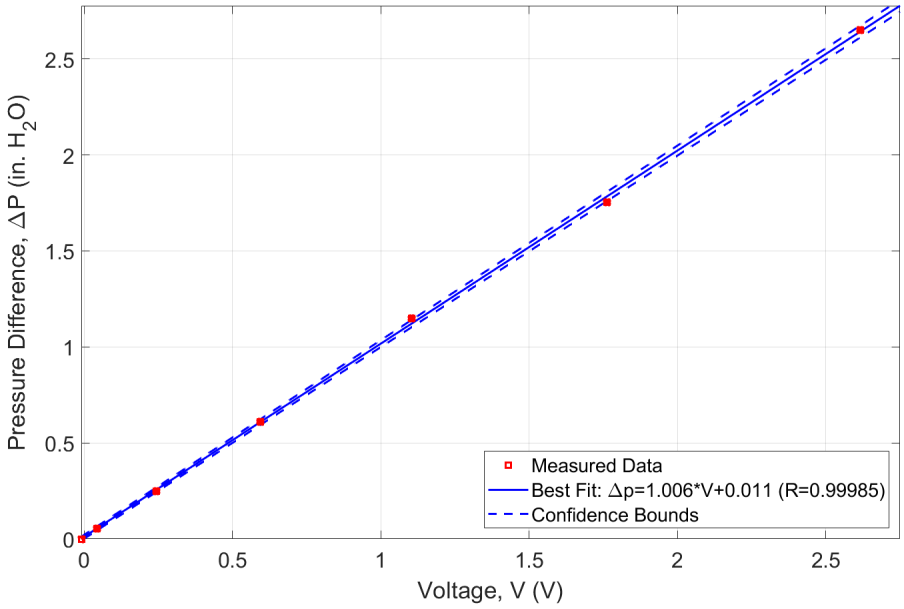

Figure 2: Pressure transducer calibration data from digital barometer and manometer.

The relationship expressed in Eq. 3 and depicted in Figure 2 was used for all future parts of the lab to convert voltage measurement to pressure difference values. These pressure differences were then converted to velocity via Bernoulli's Equation, given as

$$v = \sqrt{\frac{2\Delta P}{\rho}} \tag{4}$$

where v is the velocity measured by the pitot probe. The uncertainty in velocity measurements could be calculated via the equation

$$\epsilon_v = \sqrt{\left(\frac{\epsilon_{\Delta P}}{\rho}\sqrt{\frac{\rho}{2\Delta P}}\right)^2 + \left(\frac{\epsilon_{\Delta P}\Delta P}{\rho^2}\sqrt{\frac{\rho}{2\Delta P}}\right)^2} \tag{5}$$

where ϵ_v is the uncertainty in velocity and $\epsilon_{\Delta P}$ is the uncertainty in the pressure difference which was obtained from adding the uncertainties in the linear regression coefficients in quadrature.

4.2 Transverse of Tunnel Freestream

Data on the freestream velocity profile of the wind tunnel was acquired using the methods described in sections 3.2 and 4.1. Figure 3 depicts the freestream velocity profile of the subsonic tunnel, taken with nothing inside the tunnel to cause a wake. As reported in 3.2 Freestream Velocity Profile, the data was measured by moving the pitot probe vertically as the tunnel speed remained constant. The velocity profile in Figure 3 is plotted with error bounds calculated with Eq. 5 at each point gathered. The variation in velocity as a function of position ranges from 24.75 to 25.05 $\frac{\text{m}}{\text{s}}$ or only 0.3 $\frac{\text{m}}{\text{s}}$. Due to the small variation in freestream velocity, the scale of the y-axis in Figure 3 is rather small and the error bars are rather large, but this actually represents a relatively small standard deviation and very reasonable uncertainty. This flow profile is important both to recognize that the freestream flow in the tunnel can be considered uniform and to serve as a baseline from which drag can be calculated when an article is placed in the wind tunnel.

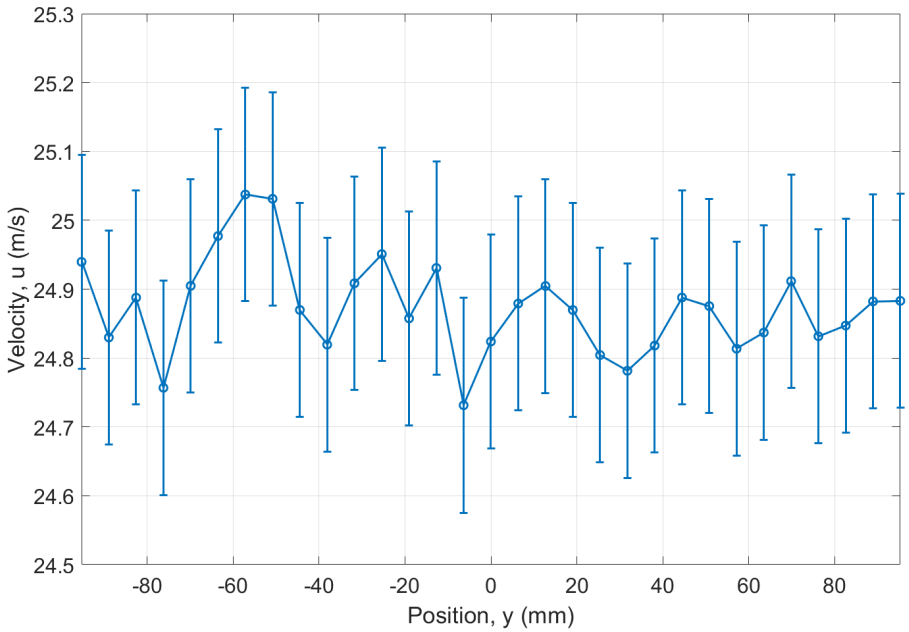

Figure 3: Freestream velocity profile subsonic tunnel measured by pitot static probe.

4.3 Cylinder and Airfoil Wake Profiles

Data on the cylinder and airfoil wake profiles were collected using the methods described in sections 3.3 and 3.4. Figure 4 shows the wake profiles of the cylinder, NACA 0015 airfoil, and the freestream velocity together with their respective error bounds calculated with Eq.

5. Each dataset was collected by measuring the velocity of the freestream by moving the pitot probe throughout the test section. The velocity remains almost constant around 25 $\frac{\text{m}}{\text{s}}$ for the freestream, whereas the wake profiles have a drastic decrease in velocity behind the bodies. The NACA 0015 airfoil saw a decrease in the flow velocity from 25 to 23.5 $\frac{\text{m}}{\text{s}}$. Verses the cylinder which dropped from 25 to 20.9 $\frac{\text{m}}{\text{s}}$.

It is important to note here that the airfoil at 0° angle of attack has a very similar number of data points but spans a much narrower region of the graph, thus making it appear much smaller than the other two plotted data sets. As mentioned in Section 3.4 of Experimental Procedure, at 0° angle of attack the NACA 0015 airfoil was tested using coarse and fine surveys, each of which spanning a different range of the test section. The data set that is plotted in Figure 4 is the fine survey, which gives more data values around the point of interest. This explains the apparent discrepancy.

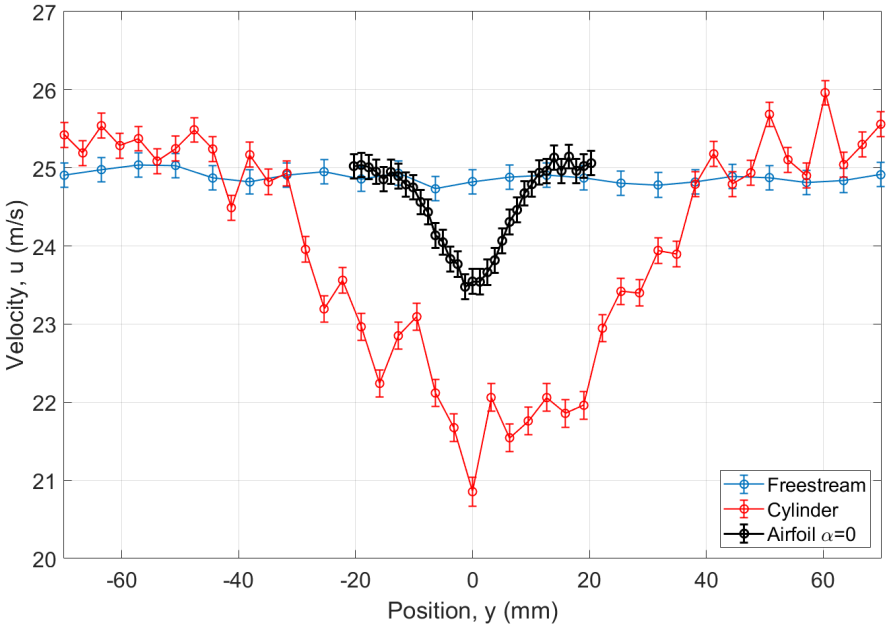

Figure 4: Wake profiles of cylindrical and NACA airfoils compared to freestream velocity.

A plot only of the NACA 0015 airfoil at different angles of attack is also very helpful for visualizing how the wake changes with those angles. Figure 5 shows the wake profile of the airfoil at 0, 5, 10, and 15 degree angles of attack with accompanying error bars at each point measured. All of the data sets plotted come from the fine survey as discussed in Section 3.4 of Experimental Procedure.

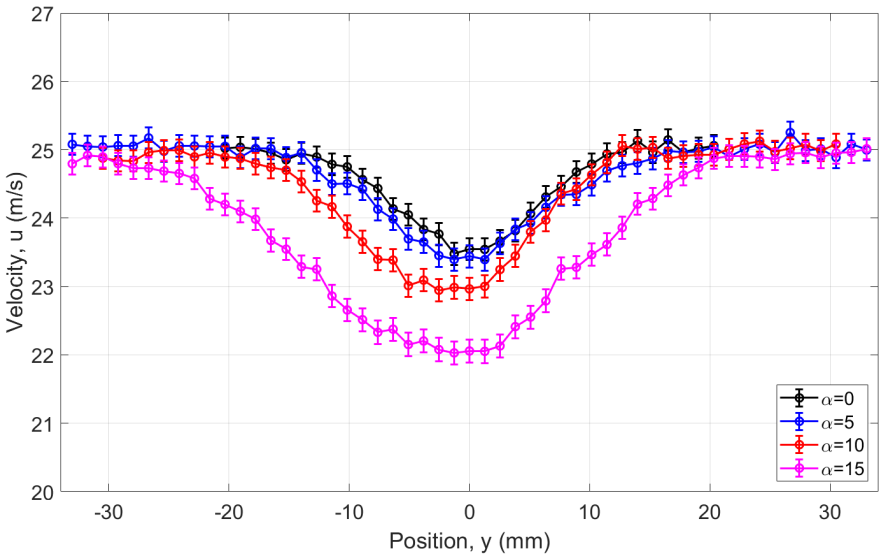

Figure 5: Wake profiles of NACA 0015 airfoil at several angles of attack

4.4 Drag Results

The dips in velocity profiles that are clearly visible in Figures 4 and 5 can be used to calculate the drag experienced by each test article by comparing those velocity profiles with a free stream profile. Specifically, the drag can be calculated via a Riemann sum integration expressed mathematically as

$$D^* = \sum_{i=1}^{N} (|y_i - y_{i-1}| \cdot (u_i \cdot (U_\infty - u_i))) \tag{6}$$

where $D^* = \frac{D'}{\rho}$, D' is the drag per unit length, N is the number of data points, y_i is the position at which the i^{th} velocity was gathered, u_i is the i^{th} velocity, and U_∞ is the freestream velocity calculated as a linear fit between the freestream velocity data at the tops and bottoms of each wake. Furthermore, the uncertainty in D^* was calculated with the equation

$$\epsilon_{D^*} = \sqrt{\left(\epsilon_\rho \frac{\partial D^*}{\partial U_\infty}\right)^2 + \left(\epsilon_u \frac{\partial D^*}{\partial u}\right)^2} \tag{7}$$

where ϵ_u is the uncertainty in the given velocity. The partial derivative in Eq. 7 are given by

$$\frac{\partial D^*}{\partial U_\infty} = \sum_{i=1}^{N} (|y_i - y_{i-1}| \cdot u_i) \tag{8}$$

and

$$\frac{\partial D^*}{\partial u} = \sum_{i=1}^{N} (|y_i - y_{i-1}| \cdot (U_\infty - 2u_i) \tag{9}$$

Finally, these parameters could be combined to calculate the uncertainty in D', the drag per unit length, which is expressed as

$$\epsilon_{D'} = \sqrt{(\epsilon_\rho D^*)^2 + (\epsilon_{D^*}\rho)^2} \tag{10}$$

In addition to knowing the drag per unit length alongside its uncertainty, it is also valuable to have a non-dimensionalized metric of drag. The drag coefficient serves this role and is calculable from the drag via the expression

$$c_D = \frac{D'}{\frac{1}{2}\rho U_\infty^2 c} \tag{11}$$

where c_D is the drag coefficient and c is the chord length in the case of the airfoils and the diameter in the case of the cylinder. Similar to the drag, the uncertainty in c_D can be calculated with the equation

$$\epsilon_{c_D} = \sqrt{\left(\epsilon_{D'}\frac{\partial c_D}{\partial D'}\right)^2 + \left(\epsilon_\rho \frac{\partial c_D}{\partial \rho}\right)^2 + \left(\epsilon_{U_\infty}\frac{\partial c_D}{\partial U_\infty}\right)^2} \tag{12}$$

where ϵ_{c_D} is the uncertainty in c_D, and the partial derivatives are given as

$$\frac{\partial c_D}{\partial D'} = \frac{1}{\frac{1}{2}\rho U_\infty^2 c} \tag{13}$$

$$\frac{\partial c_D}{\partial \rho} = \frac{-D'}{\frac{1}{2}\rho^2 U_\infty^2 c} \tag{14}$$

$$\frac{\partial c_D}{\partial U_\infty} = \frac{-2D'}{\frac{1}{2}\rho U_\infty^3 c} \tag{15}$$

It is worth noting that the entirety of the drag calculations comes from the guidance of the lab handout [2].

It is also worth noting that the values of c_D calculated by Eq. 11 are experimental values and can be compared to expected values of c_D in order to judge the quality of the experiment. Theoretical values of c_D for relevant airfoil angles of attack can be found in the lab handout. The figure cited in the handout originally came from the Subsonic Development System at MIT [3], a realistic value for the expected drag coefficient of the cylinder comes from a report issued by General Electric in conjunction with the US Air Force that reports the drag coefficient for a cylinder in the Reynold's number range experienced in this experiment's wind tunnel to be 1.200 [4].

The values of drag per unit length, drag coefficient—both experimental and expected—and the percent difference between drag coefficients are tabulated in Table 4. The "NA" in Table 4 under angle of attack references the cylinder profile. This profile cannot have any angle of attack; no matter the rotation it remains the same shape. An in-depth look at the results

summarized in Table 4 is given in Section 5.3, but a cursory glance reveals that cylinder drag is far greater than airfoil drag, though airfoil drag increases with angle of attack.

Table 4: Experimental results listing drag per unit length, and coefficients of drag at different angles of attack.

α (°)	$D'(\frac{\text{N}}{\text{m}})$	c_D Experimental	c_D Expected	% Difference
NA	5.221 ± 0.640	0.273 ± 0.034	1.200	77.3
0	0.598 ± 0.180	0.010 ± 0.003	0.010	2.28
5	0.758 ± 0.295	0.013 ± 0.005	0.015	12.9
10	0.964 ± 0.269	0.016 ± 0.005	0.024	31.7
15	1.954 ± 0.282	0.036 ± 0.005	0.049	26.9

5 Discussion

5.1 Transverse of Tunnel Freestream

As mentioned in 4.2 of Results and Analysis, the noise seen throughout the freestream test bears some discussion. The noise itself is not that large, which is expected for this scenario where the subsonic tunnel has nothing in it. However, the noise that is present may be due to a number of factors.

First, the portion of the tunnel that interfaced with the pitot probe was slotted to allow the pitot probe to move along the x-axis. This slotting opened up the top of the test section to the outside air and gave an outlet for some of the air blown through the tunnel to escape. To combat this, the open slotted portion was covered with cardboard to attempt to close off the leak, but not all of the slot was covered. This could have led to more noise. Additionally, dust and debris that were further in the tunnel than could be accessed may have contributed to nonuniform airflow as measured through the pitot probe.

Another source for the noise comes from the design of the wind tunnel itself. Using a diagram of the wind tunnel from the Lab handout [1] in Figure 1 the inlet flow can be better understood. As the tunnel is turned on, the air is pulled through the test section via the large turbine powered by a pulley and belt system. The inflow of air is designed to pass through a set of 12 fine mesh screens in hopes of breaking any large turbulence or vorticities in the flow before it gets to the testing section. The noise in the freestream flow can be a result of large vorticities in the flow that did not settle before coming into the testing section

Several improvements could be made to improve the accuracy of the test and decrease the noise and variation of the data. First, better sealing for the slotted section is necessary. The slotted section where the pitot probe meets the test section needs to have a more refined method of being closed off such that the air blown through the tunnel cannot escape. Additionally, a more thorough cleaning of the subsonic tunnel could help to eliminate any debris or obstacles that would obscure test data.

5.2 Cylinder and Airfoil Wake Profiles

The wake profile of the cylinder, airfoil, and freestream are different a thus deserve some explanation for the difference. According to Figure 4, the velocity measured by the pitot probe of the air going over the cylinder installed in the tunnel is much less than that of the air going over the airfoil. This result was expected as the cylinder acts as a bluff body in the freestream, causing a much larger wake profile to form behind it than the narrow airfoil. The noise of the cylinder dataset was a result of the rough survey done for the profile compared to the fine survey done on the airfoil. The rough profile allowed for a wider range of data collection at the cost of some accuracy that the fine survey gives.

To improve the accuracy of this data, a fine survey of the cylinder wake profile could be taken. This survey would take much longer as the step size for the fine survey was 0.05 in. However, the thickness of the airfoil is not the only factor that goes into its wake propagation. The angle of attack of the airfoil also plays a large role in the formation. From Figure 5, one can see that the velocity measured by the pitot probe over the NACA 0015 airfoil decreases as the angle of attack increases. The decrease in downstream velocity is a result of the increasing separation layer and vortices that form on the upper layer of the airfoil.

5.3 Drag Results

The percent difference between the experimental and expected coefficient of drag data must be explained further. As seen in Table 4, the largest observed c_D is from the cylinder in the subsonic tunnel, denoted by the NA angle of attack. This would make sense because the cylinder is a bluff body while the airfoils are streamlined bodies. This bluff body distinction means that a significant portion of the wake is separated flow, that it has detached from the body. The streamlined body implies that most of the flow is still attached. The experimentally gathered c_D data follows the trend of the expected c_D data in that the c_D increases as the angle of attack increases for the airfoil and that the c_D is greater for the cylinder than the airfoil.

The percent difference between experimental and expected varied greatly between the different profile shapes: with the largest difference being 77.3% with the cylinder and the smallest being a 2.28% difference for the 0 degree angle of attack airfoil. One possible explanation for the great disparity between the measured and expected c_D for the cylinder may be that the air coming in from the slotted section makes the airflow turbulent. As discussed in Section 5.1, one of the main sources of error comes from the open section of the subsonic tunnel which could cause the flow to trip from laminar to turbulent.

6 Conclusion

6.1 Summary

The Transducer Calibration and Pitot Wake Profiles lab employed the wind tunnel facilities at Hessert Laboratories in order to conduct multiple freestream experiments. Over the

course of these experiments the different test articles were placed into the test section of the tunnel in order to determine the wake profiles of different bluff and aerodynamic bodies. The aerodynamic body was a NACA 0015 which was tested at different angles of attack, showing the effect of attack angle and drag coefficient. With the data collected, the drag per unit span, drag coefficient and their respective uncertainties were calculated. The final results measured a drag force ranging from 5.221 $\frac{\text{N}}{\text{M}}$ for the circular body to 0.598 $\frac{\text{N}}{\text{M}}$ for the airfoil at zero angle of attack. Furthermore, the coefficient of drag was much higher for bluff body at 0.273 compared to 0.01.

6.2 Recommended Improvements

Overall, the experiment saw success in several areas. However, there are still multiple improvements that can be made:

- The best way that the uncertainties in all of the results could be lowered would be to gather more data. This applies specifically to the region within the wake. In the experiment, the data was spatially finer for the airfoils, but there is no reason that the data could not have been even finer. Additionally, the data for the cylinder was rather rough by comparison, and gathering more data points within its wake would have done a lot to lessen the uncertainties in its drag and drag coefficient.

- As another major source of noise within the tunnel came from the slotted portion on the top of the tunnel that interfaced with the pitot probe, another improvement could be to better seal the gaps. Creating a better seal between the outside air and the tunnel would serve to decrease any leaks from the subsonic tunnel and prevent any of the atmospheric conditions from interfering with the tests.

- Lastly, the lab and—to an even greater degree—the data analysis could have been much more efficient if the GUI for moving the pitot probe was improved. As it was, the probe was moved by specifying the number of steps and repetitions, which the user had to convert to distance. More than once, this led to confusion on how far the probe had actually been moved, and if enough data had been gathered. An improvement would be to allow the user to specify the distance the probe should be moved and then either specify the number of data points to be collected or the distance between data points.

Together these improvements would make for a smoother experiment with more robust results.

References

[1] AME30333, *Lab 1: Transducer Calibration & Pitot Wake Profiles*, University of Notre Dame, Notre Dame, IN, 2024.

[2] AME30333, *Pre-Lab Assignment 1*, University of Notre Dame, Notre Dame, IN, 2024.

[3] Drela, M., "XFOIL: Subsonic Development System," Massachusettes Institute of Technology,John Wiley. Xfoil 6.99 (Unix, Windows), Dec 23, 2013.

[4] Heddleson, C. F., *Summary of Drag Coefficients of Various Shaped Cylinders*, General Electric, Cincinnati 15, Ohio, 1957.

Appendix A - MATLAB Data Analysis Code

2/25/24 8:22 PM C:\Users\tjwel\Desktop...\dataAnalysis.m 1 of 9

```
% Lab 1 Analysis

% by Timothy Welch

clear; clc; close all

%% Load and Initialize Data
load("pressure_cal.mat")
V = mean_data; % [V]
dp = [0;0.055;0.250;0.610;1.150;1.755;2.650]; % [in. H2O]
edp = 0.005; % [in. H2O]
eV = 7e-3; % [V] 14% of range from spec sheet

%% Fit
p = polyfit(V,dp,1);
save("polyfit.mat","p")

Vtheo = linspace(V(1),2.75,1000);
Ptheo = p(1)*Vtheo+p(2);

R = corrcoef(V,dp);

%% Std. Dev. Calculations
sigmay = sqrt(ones(1,length(V))*((dp-p(2)-p(1)*V).^2)/(length(V)-2));
delta = length(V)*(dot(V,V)) - (ones(1,length(V))*V)^2;
sigmab = sigmay*sqrt(dot(V,V)/delta);
sigmaa = sigmay*sqrt(length(V)/delta);
disp("sigma_y: " + num2str(sigmay))
disp("sigma_b: " + num2str(sigmab))
disp("sigma_a: " + num2str(sigmaa))

Ptheomin = (p(1)+sigmaa)*Vtheo+(p(2)+sigmab);
Ptheomax = (p(1)-sigmaa)*Vtheo+(p(2)-sigmab);

%% Plot
figure(1)
plot(V,dp,'rsquare',Vtheo,Ptheo,'b-',Vtheo,Ptheomin,...
    'b--',Vtheo,Ptheomax,'b--','Linewidth',1.5)
hold on
errorbar(V,dp,edp,'horizontal','rsquare','Linewidth',1.5)
errorbar(V,dp,eV,'vertical','rsquare','Linewidth',1.5)
hold off
set(gca,'fontSize',16)
grid on
legend('Measured Data',"Best Fit: \Deltap="+num2str(round(p(1),3))+"*V+"...
    +num2str(round(p(2),3))+" (R="+num2str(R(1,2))+")",...
    'Confidence Bounds','Location','southeast')
xlabel('Voltage, V (V)')
ylabel('Pressure Difference, \DeltaP (in. H_2O)')
axis([Vtheo(1),Vtheo(end),0,Ptheo(end)])
```

```
%% Clear
clear

%% Load Polyfit
p = load('polyfit.mat');
a = p.p(1);
b = p.p(2);

%% Ambient Conditions
R = 287; % [J/kg/K]
Tbar = 0.5*(74.0+73.1); % [F]
T = (5/9)*(Tbar-32)+273.15; % [K] conversion from 74F
Pbar = 0.5*(29.39+29.39); % [in Hg]
P = Pbar*3386.39; % [Pa] conversion from 29.39 in Hg
eP = sqrt(100^2+400^2+100^2); % [Pa]
eT = sqrt(0.1^2+0.4^2+0.4^2); % [K]
rho = P/(R*T); % [kg/m^3]
erho = sqrt((eP/(R*T))^2+(-eT*P/(R*T^2))^2); % [kg/m^3]

%% Traverse of Tunnel Free Stream
load("tunnel-profile.mat")
load("stdevData.mat")
V = mean_data; % [V]
y = (-3.75:0.25:3.75)'*25.4; % [mm]
dp = a*V+b; % [in H2O]
eV = 7e-3; % [V] 14% of range from spec sheet

edp = sqrt((sigmaa*max(V))^2+sigmab^2+(eV*a)^2); % [in H2O]
dp = dp*248.84; % [Pa]
edp = edp*248.84; % [Pa]

v = sqrt(2*dp/rho); % [m/s]

ev = sqrt((edp*0.5*(2*dp/rho).^(-1/2).*(2/rho)).^2 ...
    +(erho*0.5*(2*dp/rho).^(-1/2).*(-2*dp/rho^2)).^2); % [m/s]

figure(2)
errorbar(y,v,ev,'-o','Linewidth',1.5);
set(gca,'fontSize',16)
grid on
xlabel('Position, y (mm)')
ylabel('Velocity, u (m/s)')
axis([25.4*-3.75,25.4*3.75,24.5,25.3])

%%  Cylinder and Airfoil Wake Profiles
load("cylinder-profile.mat")
Vcyl = mean_data(47:93); % [V]
ycyl = (-2.875:0.125:2.875)'*25.4; % [mm]
dpcyl = a*Vcyl+b; % [in H2O]
```

```
eVcyl = 7e-3; % [V] 14% of range from spec sheet

edpcyl = sqrt((sigmaa*max(Vcyl))^2+sigmab^2+(eVcyl*a)^2); % [in H2O]
dpcyl = dpcyl*248.84; % [Pa]
edpcyl = edpcyl*248.84; % [Pa]

vcyl = sqrt(2*dpcyl/rho); % [m/s]

evcyl = sqrt((edpcyl*0.5*(2*dpcyl/rho).^(-1/2).*(2/rho)).^2 ...
    +(erho*0.5*(2*dpcyl/rho).^(-1/2).*(-2*dpcyl/rho^2)).^2); % [m/s]

load("airfoil_profile_0_fine.mat")
V0 = mean_data(33:end); % [V]
y0 = (-0.8:0.05:0.8)'*25.4; % [mm]
dp0 = a*V0+b; % [in H2O]
eV0 = 7e-3; % [V] 14% of range from spec sheet

edp0 = sqrt((sigmaa*max(V0))^2+sigmab^2+(eV0*a)^2); % [in H2O]
dp0 = dp0*248.84; % [Pa]
edp0 = edp0*248.84; % [Pa]

v0 = sqrt(2*dp0/rho); % [m/s]

ev0 = sqrt((edp0*0.5*(2*dp0/rho).^(-1/2).*(2/rho)).^2 ...
    +(erho*0.5*(2*dp0/rho).^(-1/2).*(-2*dp0/rho^2)).^2); % [m/s]

figure(3)
errorbar(y,v,ev,'-o','Linewidth',1);
hold on
errorbar(ycyl,vcyl,evcyl,'r-o','Linewidth',1);
errorbar(y0,v0,ev0,'k-o','Linewidth',1.5);
hold off
legend('Freestream','Cylinder','Airfoil \alpha=0','Location','southeast')
set(gca,'fontSize',16)
grid on
xlabel('Position, y (mm)')
ylabel('Velocity, u (m/s)')
axis([-70,70,20,27])

%%  Airfoil Angles of Attack Wake Profiles
load("airfoil_profile_0_fine.mat")
V0 = mean_data(33:end); % [V]
y0 = (-0.8:0.05:0.8)'*25.4; % [mm]
dp0 = a*V0+b; % [in H2O]
eV0 = 7e-3; % [V] 14% of range from spec sheet

edp0 = sqrt((sigmaa*max(V0))^2+sigmab^2+(eV0*a)^2); % [in H2O]
dp0 = dp0*248.84; % [Pa]
edp0 = edp0*248.84; % [Pa]
```

```
v0 = sqrt(2*dp0/rho); % [m/s]

ev0 = sqrt((edp0*0.5*(2*dp0/rho).^(-1/2).*(2/rho)).^2 ...
    +(erho*0.5*(2*dp0/rho).^(-1/2).*(-2*dp0/rho^2)).^2); % [m/s]

load("airfoil_profile_5.mat")
V5 = mean_data(33:end); % [V]
y5 = (-1.3:0.05:1.3)'*25.4; % [mm]
dp5 = a*V5+b; % [in H2O]
eV5 = 7e-3; % [V] 14% of range from spec sheet

edp5 = sqrt((sigmaa*max(V5))^2+sigmab^2+(eV5*a)^2); % [in H2O]
dp5 = dp5*248.84; % [Pa]
edp5 = edp5*248.84; % [Pa]

v5 = sqrt(2*dp5/rho); % [m/s]

ev5 = sqrt((edp5*0.5*(2*dp5/rho).^(-1/2).*(2/rho)).^2 ...
    +(erho*0.5*(2*dp5/rho).^(-1/2).*(-2*dp5/rho^2)).^2); % [m/s]

load("airfoil_profile_10.mat")
V10 = mean_data(1:end-11); % [V]
y10 = (-1.2:0.05:1.2)'*-25.4; % [mm]
dp10 = a*V10+b; % [in H2O]
eV10 = 7e-3; % [V] 14% of range from spec sheet

edp10 = sqrt((sigmaa*max(V10))^2+sigmab^2+(eV10*a)^2); % [in H2O]
dp10 = dp10*248.84; % [Pa]
edp10 = edp10*248.84; % [Pa]

v10 = sqrt(2*dp10/rho); % [m/s]

ev10 = sqrt((edp10*0.5*(2*dp10/rho).^(-1/2).*(2/rho)).^2 ...
    +(erho*0.5*(2*dp10/rho).^(-1/2).*(-2*dp10/rho^2)).^2); % [m/s]

load("airfoil_profile_15.mat")
V15 = mean_data(18:end); % [V]
y15 = (-1.3:0.05:1.3)'*25.4; % [mm]
dp15 = a*V15+b; % [in H2O]
eV15 = 7e-3; % [V] 14% of range from spec sheet

edp15 = sqrt((sigmaa*max(V15))^2+sigmab^2+(eV15*a)^2); % [in H2O]
dp15 = dp15*248.84; % [Pa]
edp15 = edp15*248.84; % [Pa]

v15 = sqrt(2*dp15/rho); % [m/s]

ev15 = sqrt((edp15*0.5*(2*dp15/rho).^(-1/2).*(2/rho)).^2 ...
    +(erho*0.5*(2*dp15/rho).^(-1/2).*(-2*dp15/rho^2)).^2); % [m/s]
```

```
figure(4)
errorbar(y0,v0,ev0,'k-o','Linewidth',1.5);
hold on
errorbar(y5,v5,ev5,'b-o','Linewidth',1.5);
errorbar(y10,v10,ev10,'r-o','Linewidth',1.5);
errorbar(y15,v15,ev15,'m-o','Linewidth',1.5);
hold off
legend('\alpha=0','\alpha=5','\alpha=10','\alpha=15','Location','southeast')
set(gca,'fontSize',16)
grid on
xlabel('Position, y (mm)')
ylabel('Velocity, u (m/s)')
axis([-34,34,20,27])

%% Drag Calculations
Uinf = {linspace(mean([vcyl(1),vcyl(2),vcyl(3)]),...
        mean([vcyl(end),vcyl(end-1),vcyl(end-2)]),length(vcyl));...
        linspace(mean([v0(1),v0(2),v0(3)]),...
        mean([v0(end),v0(end-1),v0(end-2)]),length(v0));...
        linspace(mean([v5(1),v5(2),v5(3)]),...
        mean([v5(end),v5(end-1),v5(end-2)]),length(v5));...
        linspace(mean([v10(1),v10(2),v10(3)]),...
        mean([v10(end),v10(end-1),v10(end-2)]),length(v10));...
        linspace(mean([v15(1),v15(2),v15(3)]),...
        mean([v15(end),v15(end-1),v15(end-2)]),length(v15))};

% Cylinder
Dstar = 0; %[m^3/s^2] (D`/rho)
pDstarpUinf = 0;
pDstarpu = 0;
c = 2/39.37; % [m]
ycyl = ycyl/1000; % [m]

for i=2:length(vcyl)
    Dstar = Dstar + abs(ycyl(i)-ycyl(i-1))*vcyl(i)*(Uinf{1}(i)-vcyl(i));
    pDstarpUinf = pDstarpUinf + abs((ycyl(i)-ycyl(i-1)))*vcyl(i);
    pDstarpu = pDstarpu + abs((ycyl(i)-ycyl(i-1)))*(Uinf{1}(i)-2*vcyl(i));
end

eDstar = sqrt((erho*pDstarpUinf)^2+(mean(evcyl)*pDstarpu)^2);
Dprime = Dstar*rho;
eDprime = sqrt((erho*Dstar)^2+(eDstar*rho)^2);

cd = 2*Dprime/(rho*mean(Uinf{1})^2*c);

pcdpDprime = 2/(rho*mean(Uinf{1})^2*c);
pcdprho = -2*Dprime/(rho^2*mean(Uinf{1})^2*c);
pcdpuinf = -4*Dprime/(rho*mean(Uinf{1})^3*c);

ecd = sqrt((eDprime*pcdpDprime)^2+(erho*pcdprho)^2+(mean(ev)*pcdpuinf)^2);
```

```
D(1) = Dprime; eD(1) = eDprime; cD(1) = cd; ecD(1) = ecd;

% Airfoil 0
Dstar = 0; %[m^3/s^2] (D`/rho)
pDstarpUinf = 0;
pDstarpu = 0;
c = 6/39.37; % [m]
y0 = y0/1000; % [m]

for i=2:length(v0)
    Dstar = Dstar + abs(y0(i)-y0(i-1))*v0(i)*(Uinf{2}(i)-v0(i));
    pDstarpUinf = pDstarpUinf + abs((y0(i)-y0(i-1)))*v0(i);
    pDstarpu = pDstarpu + abs((y0(i)-y0(i-1)))*(Uinf{2}(i)-2*v0(i));
end

eDstar = sqrt((erho*pDstarpUinf)^2+(mean(ev0)*pDstarpu)^2);
Dprime = Dstar*rho;
eDprime = sqrt((erho*Dstar)^2+(eDstar*rho)^2);

cd = 2*Dprime/(rho*mean(Uinf{2})^2*c);

pcdpDprime = 2/(rho*mean(Uinf{2})^2*c);
pcdprho = -2*Dprime/(rho^2*mean(Uinf{2})^2*c);
pcdpuinf = -4*Dprime/(rho*mean(Uinf{2})^3*c);

ecd = sqrt((eDprime*pcdpDprime)^2+(erho*pcdprho)^2+(mean(ev)*pcdpuinf)^2);

D(2) = Dprime; eD(2) = eDprime; cD(2) = cd; ecD(2) = ecd;

% Airfoil 5
Dstar = 0; %[m^3/s^2] (D`/rho)
pDstarpUinf = 0;
pDstarpu = 0;
c = 6/39.37; % [m]
y5 = y5/1000; % [m]

for i=2:length(v5)
    Dstar = Dstar + abs(y5(i)-y5(i-1))*v5(i)*(Uinf{3}(i)-v5(i));
    pDstarpUinf = pDstarpUinf + abs((y5(i)-y5(i-1)))*v5(i);
    pDstarpu = pDstarpu + abs((y5(i)-y5(i-1)))*(Uinf{3}(i)-2*v5(i));
end

eDstar = sqrt((erho*pDstarpUinf)^2+(mean(ev5)*pDstarpu)^2);
Dprime = Dstar*rho;
eDprime = sqrt((erho*Dstar)^2+(eDstar*rho)^2);

cd = 2*Dprime/(rho*mean(Uinf{3})^2*c);

pcdpDprime = 2/(rho*mean(Uinf{3})^2*c);
```

```
pcdprho = -2*Dprime/(rho^2*mean(Uinf{3})^2*c);
pcdpuinf = -4*Dprime/(rho*mean(Uinf{3})^3*c);

ecd = sqrt((eDprime*pcdpDprime)^2+(erho*pcdprho)^2+(mean(ev)*pcdpuinf)^2);

D(3) = Dprime; eD(3) = eDprime; cD(3) = cd; ecD(3) = ecd;

% Airfoil 10
Dstar = 0; %[m^3/s^2] (D`/rho)
pDstarpUinf = 0;
pDstarpu = 0;
c = 6/39.37; % [m]
y10 = y10/1000; % [m]

for i=2:length(v10)
    Dstar = Dstar + abs(y10(i)-y10(i-1))*v10(i)*(Uinf{4}(i)-v10(i));
    pDstarpUinf = pDstarpUinf + abs((y10(i)-y10(i-1)))*v10(i);
    pDstarpu = pDstarpu + abs((y10(i)-y10(i-1)))*(Uinf{4}(i)-2*v10(i));
end

eDstar = sqrt((erho*pDstarpUinf)^2+(mean(ev10)*pDstarpu)^2);
Dprime = Dstar*rho;
eDprime = sqrt((erho*Dstar)^2+(eDstar*rho)^2);

cd = 2*Dprime/(rho*mean(Uinf{4})^2*c);

pcdpDprime = 2/(rho*mean(Uinf{4})^2*c);
pcdprho = -2*Dprime/(rho^2*mean(Uinf{4})^2*c);
pcdpuinf = -4*Dprime/(rho*mean(Uinf{4})^3*c);

ecd = sqrt((eDprime*pcdpDprime)^2+(erho*pcdprho)^2+(mean(ev)*pcdpuinf)^2);

D(4) = Dprime; eD(4) = eDprime; cD(4) = cd; ecD(4) = ecd;

% Airfoil 15
Dstar = 0; %[m^3/s^2] (D`/rho)
pDstarpUinf = 0;
pDstarpu = 0;
c = 6/39.37; % [m]
y15 = y15/1000; % [m]

for i=2:length(v15)
    Dstar = Dstar + abs(y15(i)-y15(i-1))*v15(i)*(Uinf{5}(i)-v15(i));
    pDstarpUinf = pDstarpUinf + abs((y15(i)-y15(i-1)))*v15(i);
    pDstarpu = pDstarpu + abs((y15(i)-y15(i-1)))*(Uinf{5}(i)-2*v15(i));
end

eDstar = sqrt((erho*pDstarpUinf)^2+(mean(ev15)*pDstarpu)^2);
Dprime = Dstar*rho;
eDprime = sqrt((erho*Dstar)^2+(eDstar*rho)^2);
```

```
cd = 2*Dprime/(rho*mean(Uinf{5})^2*c);

pcdpDprime = 2/(rho*mean(Uinf{5})^2*c);
pcdprho = -2*Dprime/(rho^2*mean(Uinf{5})^2*c);
pcdpuinf = -4*Dprime/(rho*mean(Uinf{5})^3*c);

ecd = sqrt((eDprime*pcdpDprime)^2+(erho*pcdprho)^2+(mean(ev)*pcdpuinf)^2);

D(5) = Dprime; eD(5) = eDprime; cD(5) = cd; ecD(5) = ecd;

%% Final Calculations
cDtheo = [1.2,0.010,0.015,0.024,0.049];
perDiff = abs(cDtheo-cD)./cDtheo*100;

%% Table to LaTex
T = array2table([D',eD',cD',ecD',cDtheo',perDiff']);
table2latex(T,'lab1DragData')

function table2latex(T, filename)

    % Error detection and default parameters
    if nargin < 2
        filename = 'table.tex';
        fprintf('Output path is not defined. The table will be written in %s.\n',↙
filename);
    elseif ~ischar(filename)
        error('The output file name must be a string.');
    else
        if ~strcmp(filename(end-3:end), '.tex')
            filename = [filename '.tex'];
        end
    end
    if nargin < 1, error('Not enough parameters.'); end
    if ~istable(T), error('Input must be a table.'); end

    % Parameters
    n_col = size(T,2);
    col_spec = [];
    for c = 1:n_col, col_spec = [col_spec 'l']; end
    col_names = strjoin(T.Properties.VariableNames, ' & ');
    row_names = T.Properties.RowNames;
    if ~isempty(row_names)
        col_spec = ['l' col_spec];
        col_names = ['& ' col_names];
    end

    % Writing header
    fileID = fopen(filename, 'w');
    fprintf(fileID, '\\begin{tabular}{%s}\n', col_spec);
```

```
    fprintf(fileID, '%s \\\\ \n', col_names);
    fprintf(fileID, '\\hline \n');

    % Writing the data
    try
        for row = 1:size(T,1)
            temp{1,n_col} = [];
            for col = 1:n_col
                value = T{row,col};
                if isstruct(value), error('Table must not contain structs.'); end
                while iscell(value), value = value{1,1}; end
                if isinf(value), value = '$\infty$'; end
                temp{1,col} = num2str(value);
            end
            if ~isempty(row_names)
                temp = [row_names{row}, temp];
            end
            fprintf(fileID, '%s \\\\ \n', strjoin(temp, ' & '));
            clear temp;
        end
    catch
        error('Unknown error. Make sure that table only contains chars, strings or↙
numeric values.');
    end

    % Closing the file
    fprintf(fileID, '\\hline \n');
    fprintf(fileID, '\\end{tabular}');
    fclose(fileID);
end
```